


## Dispersive effects in ultrafast nonlinear phenomena: The case of optical Kerr effect

Dusan Lorenc and Zhanybek Alpichshev <sup>\*</sup>

*Institute of Science and Technology Austria, Am Campus 1, 3400 Klosterneuburg, Austria*

 (Received 14 June 2023; revised 23 August 2023; accepted 27 November 2023; published 11 January 2024)

It is a basic principle that an effect cannot come before the cause. Dispersive relations that follow from this fundamental fact have proven to be an indispensable tool in physics and engineering. They are most powerful in the domain of linear response where they are known as Kramers-Kronig relations. However, when it comes to nonlinear phenomena the implications of causality are much less explored, apart from several notable exceptions. Here in this paper we demonstrate how to apply the dispersive formalism to analyze the ultrafast nonlinear response in the context of the paradigmatic nonlinear Kerr effect. We find that the requirement of causality introduces a noticeable effect even under assumption that Kerr effect is mediated by quasi-instantaneous off-resonant electronic hyperpolarizability. We confirm this by experimentally measuring the time-resolved Kerr dynamics in GaAs by means of a hybrid pump-probe Mach-Zehnder interferometer and demonstrate the presence of an intrinsic lagging between amplitude and phase responses as predicted by dispersive analysis. Our results describe a general property of the time-resolved nonlinear processes thereby highlighting the importance of accounting for dispersive effects in the nonlinear optical processes involving ultrashort pulses.

DOI: [10.1103/PhysRevResearch.6.013042](https://doi.org/10.1103/PhysRevResearch.6.013042)

### I. INTRODUCTION

The amazing developments in ultrafast laser technology of the past few decades have now enabled probing materials at the unprecedented timescales down to those associated with quantum transition times between the stationary atomic states [1]. All the more important in these extreme regimes is to remain mindful of fundamental limitations imposed on the material response, both linear and nonlinear, by the basic physical principles. In the present paper we explore the implications of causality on ultrafast nonlinear optical response in the context of the paradigmatic Kerr effect (KE), whereby the refractive index experienced by a probing beam depends on the intensity of light. This effect is one of the most important nonlinear optical effects, responsible for a great number of practically important phenomena such as self- and cross-phase modulation of the beams, Kerr lensing, self-focusing, optical soliton formation, optical switching, and passive mode locking [2,3]. Since most of these become particularly prominent in the context of ultrashort laser pulses, it can be said that Kerr effect owes most of its relevance to the fact that it can be often treated as an almost instantaneous interaction between the probing pulse and the pumping one, responsible for the refractive index changes.

The mechanism of fast Kerr effect relies on off-resonant electronic transitions whose characteristic response times can be as short as several femtoseconds [2,4]. However, as we argue below, it would be a mistake to assume that quasi-

instantaneous electronic response necessarily implies that the actual response of the probing beam to the pump intensity variations is also instantaneous. The reason for this is causality [5], which inevitably leads to the dispersion of response functions [6]. This relation has been originally realized in the form of celebrated Kramers-Kronig relations [7,8] and has since found applications in a broad array of subjects in physics [9–14] and engineering [15]. Unfortunately despite general character of the relationship between causality and frequency dependence of response, the applications of dispersive analysis in nonlinear phenomena has been comparatively limited, save for several notable exceptions such as [16–19].

In the present paper we consider the Kerr effect mediated by quasi-instantaneous off-resonant electronic cloud polarization and show how to consistently apply Kramers-Kronig relations with time-dependent intensity  $I(t)$ . We apply this approach to the case of two Gaussian pulses and demonstrate that dispersion introduces a considerable lag between the phase- and amplitude response of the probe. This lag is readily measurable with ultrafast pulses, therefore we proceed with an experimental realization in a time-resolved Mach-Zehnder interferometer in the model system GaAs. We confirm the presence of the dispersive lag with the magnitude and sign of the effect being consistent with theoretical expectations.

### II. DISPERSIVE ANALYSIS OF TIME-RESOLVED KERR EFFECT

The essence of Kerr effect is the modification of linear refractive index of the given material in response to the square of applied electric field. In the case of optical frequency fast alternating applied field, the correction  $\delta n$  to the refractive index is proportional to the intensity  $I$  of the optical beam:  $\delta n = n_2 I$ , where the coefficient  $n_2$  is referred to as either Kerr or nonlinear refractive index. The realization that the end

<sup>\*</sup>alpishev@ist.ac.at

*Published by the American Physical Society under the terms of the Creative Commons Attribution 4.0 International license. Further distribution of this work must maintain attribution to the author(s) and the published article's title, journal citation, and DOI.*

result of this *nonlinear* phenomenon (KE) is a correction to a *linear* response function (refractive index) has enabled a quantitative analysis of Kerr effect in terms of the classical Kramers-Kronig relations [16,17]. In particular, it was noted that when the intensity  $I$  is constant, the refractive index acquires a constant correction, which is usual Kramers-Kronig relations, automatically applies to the frequency dependence of the nonlinear refractive index  $n_2(\omega)$ .

In many applications, however, one often deals with time-dependent, pulse-shaped intensity profiles  $I(t)$ . In this case the analysis of the Kerr effect is not as straightforward anymore [e.g., one obviously cannot simply write  $\delta n(t) = n_2 I(t)$ ]. The goal of this section is to extend the dispersive analysis of Kerr effect of Sheik-Bahae *et al.* [16,17] to the case of ultrafast pulses. Although in many practical instances KE manifests itself the self interaction of a single beam, it is convenient to think about KE as an interaction between two distinct beams: pump and probe. Then KE can be viewed as the change in effective refractive index, experienced by probe beam  $E_{\text{pr}}$ , by the presence of the pump intensity  $I_p$ . For the purposes of this paper we will ignore the spatial walk-off between the pump and probe beams due to group velocity dispersion. This can be justified for the case of thin sample or sufficiently close wavelength values of the two beams. Effectively this implies that we can ignore the spatial dispersion of light inside the sample. As demonstrated in the Appendix, this is a valid assumption for the experimental settings used in this paper.

In the absence of spatial dispersion the general third-order nonlinear response of a system  $\delta E_{\text{NL}}$  can be related to the incident (probe) field  $E(t)$  by means of a generic response function  $\bar{\chi}^{(3)}$ ,

$$\delta E_{\text{NL}}(t) = \int_{-\infty}^t dt_1 dt_2 dt_3 \bar{\chi}^{(3)}(t; t_1, t_2, t_3) E(t_1) E(t_2) E(t_3). \quad (1)$$

To remind, in this paper we limit our scope to the case of Kerr effect: A special case of the general third-order nonlinearity where the phase and amplitude of probe field  $E_{\text{pr}}(t)$  are modified in the presence of intensity of light  $I_p(t)$ , which, generally speaking, is time dependent. In Kerr effect, the probe in a certain sense is oblivious to the phase of the pump beam. This sets KE apart from other third order nonlinear processes such as third harmonic generation or four-wave mixing. In this case we can simplify the equation above by introducing Kerr susceptibility  $\chi^K$  as follows:

$$\delta E_{\text{NL}}(t) = \int_{-\infty}^t dt' E_{\text{pr}}(t') \int_{-\infty}^t dt'' \chi^K(t, t', t'') I_p(t''). \quad (2)$$

This dependence can be further simplified if Kerr response can be treated as instantaneous. This is approximately the case for the Kerr effect mediated by off-resonant electronic transitions, where response time of electrons  $\tau_{\text{res}}$  is on the order of  $\tau_{\text{res}} \sim h/\Delta_{\text{gap}}$ , where  $\Delta_{\text{gap}}$  is the band gap. The latter typically has a value on the order of 1 eV, which makes  $\tau_{\text{res}} \sim 4$  fs, which is much shorter than the usual width of ultrafast pulses. If the main nonlinear interaction channel in the medium is the cooperative effect of pump and probe beams (such as 2PA or Raman effect), the nonlinear Kerr susceptibility  $\chi^K$  can be

written as

$$\chi^K(t, t', t'') = f(t - t') \delta(t' - t'') \quad (3)$$

where  $f(t)$  is a certain function to be determined. The justification for this representation is that in the absence of real (on-shell) intermediate excitations, the nonlinear interaction between pump and probe can only be present when the both overlap in time. For a pump pulse of duration  $\tau_{\text{pump}}$  and frequency  $\Omega$  the relative error introduced by this ‘‘instantaneous’’ approximation can be estimated as  $\sim e^{-(\Delta_{\text{gap}} - \hbar\Omega)\tau_{\text{pump}}}$ . Now since  $\chi^K(t, t', t'') = \chi^K(t - t', t - t'') = 0$  whenever  $t'$  or  $t''$  precede  $t$ ,  $f(t) = 0$  for  $t < 0$ . This means  $f(t)$  is a causal function, and as such its Fourier transform must satisfy Kramers-Kronig relations. The equations above can be used to describe the Kerr effect with time-dependent pump intensity  $I_p(t)$  as long as it does not vary too fast [ $1/I_p (\partial I_p / \partial t) < \Delta_{\text{gap}} / \hbar$ ]. This condition is satisfied automatically whenever pump pulse can be described using slowly varying envelope approximation.

This way we reduce the full nonlinear susceptibility  $\chi^{(3)}$  to a function of single variable  $f(t)$ . Importantly  $f(t) = 0$ , whenever  $t < 0$ , therefore it must be subject to Kramers-Kronig relations. In fact, the function  $f(t)$  is directly related to the general nonlinear Kerr index  $\bar{n}_2(\omega, \Omega)$ , which describes the modification of the refractive index experienced by the probe with frequency  $\omega$  in the presence of pump radiation with frequency  $\Omega$ ,

$$f(\omega) = \int dt e^{i\omega t} f(t) \approx i(\omega L/c) \bar{n}_2(\omega, \Omega). \quad (4)$$

Combined Eqs. (2), (3), and (4) describe how to use dispersive relations with time-dependent pump intensity  $I_p(t)$ . As an example we can compute  $\delta E_{\text{NL}}$  for the case of Gaussian-shaped pump and probe pulses,

$$E_{\text{pr}}(t) = E_0 e^{-t^2/\tau^2} \cos(\Omega t), \quad I_p(t) = I_0 e^{-2(t-t_0)^2/\tau_1^2}$$

where  $\tau$  and  $\tau_1$  are durations of the probe and pump pulses respectively. The modification of the (complex) refractive index of the medium implies that the phase and amplitude of the transmitted beam will acquire a change in phase  $\Delta\phi$  and amplitude  $\Delta A$  encoded in  $\delta E_{\text{NL}}$ . One can show that, as a function of delay  $t_0$  between the pump and probe pulses, the amplitude and phase response will read

$$\begin{aligned} \Delta A &\propto -I_0 \text{Im}\{\bar{n}_2\} \exp\left[-\frac{1}{\tilde{\tau}^2} \left(t_0 - \frac{\partial \text{Re}\{\bar{n}_2\}/\partial \omega}{2 \text{Im}\{\bar{n}_2}\}\right)^2\right], \\ \Delta \phi &\propto I_0 \text{Re}\{\bar{n}_2\} \exp\left[-\frac{1}{\tilde{\tau}^2} \left(t_0 + \frac{\partial \text{Im}\{\bar{n}_2\}/\partial \omega}{2 \text{Re}\{\bar{n}_2}\}\right)^2\right], \end{aligned} \quad (5)$$

where  $\tilde{\tau}^2 = (\tau^2 + \tau_1^2)/2$ . According to these expressions, the dispersion of  $\bar{n}_2$  produces a lag between the phase and amplitude response,

$$\delta T(\omega, \Omega) = \frac{1}{2} \left[ \frac{\partial \text{Re}\{\bar{n}_2\}/\partial \omega}{\text{Im}\{\bar{n}_2\}} + \frac{\partial \text{Im}\{\bar{n}_2\}/\partial \omega}{\text{Re}\{\bar{n}_2\}} \right]. \quad (6)$$

The important feature of this lag is that it only depends on the dispersion of Kerr index  $\bar{n}_2(\omega, \Omega)$  and is independent of pump intensity magnitude  $I_0$ . To find  $\delta T(\omega, \Omega)$  we take

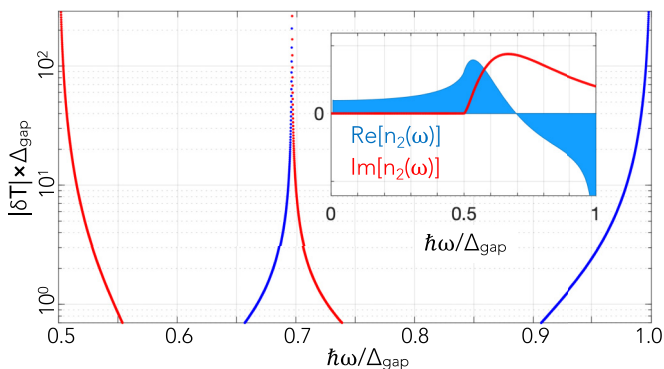


FIG. 1. Absolute value of phase-amplitude lag  $|\delta T|$  in the units of  $h/\Delta_g$  as a function of frequency as calculated from Eq. (6). Red (blue) segments correspond to positive (negative) lag with phase response lagging behind (ahead) of amplitude response. Inset: real (blue) and imaginary (red) parts of the degenerate nonlinear Kerr index  $\bar{n}_2(\omega, \Omega = \omega)$  (see Refs. [16,17]).

the complex  $\bar{n}_2(\omega, \Omega)$  as obtained by dispersive analysis assuming  $\text{Im}\{\bar{n}_2\}$  is mostly due to two-photon absorption (2PA) [16,17]. In Fig. 1 we plot “degenerate”  $\delta T$  taken at  $\omega = \Omega$ . For reference we also plot the degenerate  $\bar{n}_2(\omega, \Omega = \omega)$  in the inset of Fig. 1. As is evident from this figure, the lag is most prominent near one- and two-photon resonances. These frequencies correspond to special points  $\bar{n}_2(\omega, \Omega)$  in the complex plane  $\omega$ . Somewhat less expected is the significant lag around  $\hbar\omega \approx 0.7\Delta_{\text{gap}}$ , which corresponds to the zero-crossing of  $\text{Re}\{\bar{n}_2\}$  (inset in Fig. 1). Overall the analysis demonstrates that the lag  $\delta T$  is quite significant especially near certain special points, therefore we are turning now to its experimental observation.

### III. EXPERIMENT

In order to experimentally observe the lagging effect, we study GaAs where Kerr effect is known to be dominated by electronic hyperpolarizability [4]. To measure the nonlinear refractive index in a time-resolved manner we construct a pump-probe setup based on a Mach-Zehnder interferometer (MZI) as shown in Fig. 2(a). Here one arm of the interferometer is the probe beam that passes through the GaAs sample, while the other is used a reference. Both beams are then combined on CCD matrix of a digital camera that records the interferogram. Pump is a separate beam with a slightly different wavelength and tunable delay  $t_0$  with respect to probe. Changes in the real and imaginary parts of the refractive index induced by the pump, are recorded as respective changes in the position and amplitude of the interference pattern on the CCD matrix,

$$I(\mathbf{r}, t) \propto |E_{\text{pr}}||E_{\text{ref}}| \cos(\mathbf{q} \cdot \mathbf{r} + \phi_g + 2\pi n(t_0)L/\lambda), \quad (7)$$

here  $|E_{\text{pr}}|$  and  $|E_{\text{ref}}|$  are the amplitudes of the electric field in the probe and reference arms;  $\mathbf{q} = \mathbf{k}_1 - \mathbf{k}_2$  is the difference between the corresponding beams’ wave vectors  $\mathbf{k}_1$  and  $\mathbf{k}_2$ ;  $\phi_g$  is the static phase difference determined by interferometer geometry; and  $\mathbf{r}$  is the real-space coordinate on the surface of CCD matrix. The last term is the phase accumulated inside the sample with a thickness  $L$  and refractive index  $n$ , which

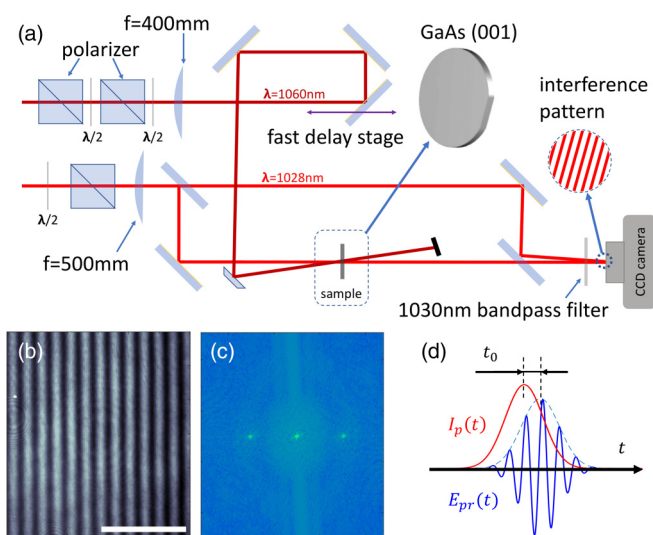


FIG. 2. (a) Schematic layout of the time-resolved Mach-Zehnder interferometer. Pump and probe beams are near-degenerate ( $\lambda = 1060$  nm and 1028 nm respectively). Transient pump-induced changes in refractive index are detected as shift in the interference pattern recorded by a CCD camera. (b) Sample interferogram as recorded by CCD camera. (c) 2D Fourier intensity of the interferogram in (b). The real-space shift of the interference pattern is inferred from the change of the phase of complex amplitude at the peak. (d) A schematic depiction of pump and probe pulses overlapping in time.

is in general a complex number. To extract the phase and amplitude information, we Fourier transform each interferogram and evaluate the complex amplitude of the Fourier peak corresponding to the main peak in the interference pattern [Figs. 2(b) and 2(c)]  $K(t_0) = |K(t_0)|e^{i\phi(t_0)}$  for each pump-probe delay  $t_0$ . The change in the absolute value and phase provide a direct measure of the pump-induced change in imaginary and real part of the refractive index.

The time dependence of pump-induced changes in phase and amplitude of the transmitted beam is shown in Fig. 3. In Fig. 3(a) the pump and probe are polarized parallel to the [100] crystalline axis of GaAs (“xx” configuration) and in Fig. 3(b) they are crossed (“xy”). The phase shift indicates that nonlinear Kerr index two distinct components: a fast peak and a slowly growing “tail”. The quasi-instantaneous character of the peak points towards off-resonant electronic polarizability as its origin, unlike the tail, which will be discussed later. Using phase shift and sample thickness  $L$  we can define an effective refractive index change as  $\bar{\delta n} = \Delta\phi/2\pi \cdot \lambda/L$ . Due to slight wavelength mismatch between pump and probe, this effective index cannot be directly used to accurately evaluate the Kerr index; however, it can still provide a reasonable estimate. With this in mind we plot  $\bar{\delta n}$  against peak pump intensity in Fig. 4(a) to find the values for the effective nonlinear Kerr index in both  $xx$  and  $xy$  configurations:  $\bar{n}_2^{xx} = (-2.8 \pm 0.5) \times 10^{-15} \text{ cm}^2/\text{W}$ ;  $\bar{n}_2^{xy} = (-1.5 \pm 0.3) \times 10^{-15} \text{ cm}^2/\text{W}$ . Numeric simulations indicate that these numbers underestimate the actual Kerr indices by about a factor of 2. Comparing these estimates against  $n_2$  values measured at other wavelengths with similar pulse duration {e.g.,  $n_2(\lambda = 1.7 \mu\text{m}) \approx 3 \times 10^{-13} \text{ cm}^2/\text{W}$  [20]} shows that our working wavelengths  $\lambda \approx 1 \mu\text{m}$  are close to the zero-crossing

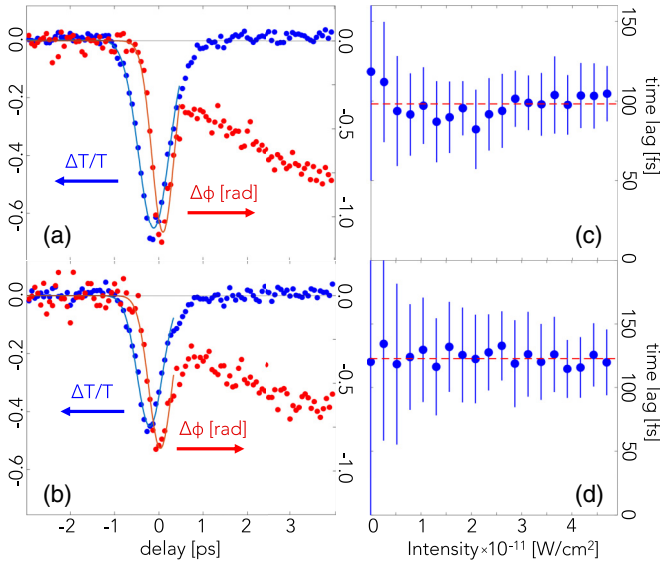


FIG. 3. (a) Pump-induced amplitude (blue) and phase (red) change as a function of pump-probe delay for  $xx$  configuration at  $I_0 = 4.7 \text{ W/cm}^2$ . Solid lines: Gaussian fits to the peaks of corresponding colors and (b) the same for  $xy$  configuration. (c) The phase-amplitude lag as a function of intensity  $I_0$  is the  $xx$  and (d)  $xy$  configurations.

value of  $\text{Re}\{\bar{n}_2\}$ , which implies that one should expect to see a significant lagging effect [see Eq. (6)].

Amplitude response  $\Delta A$  is directly related to the transient differential absorption  $\Delta T/T$  plotted in Figs. 3(a) and 3(b) in blue. Similarly to the main peak in phase response,  $\Delta T/T$  exhibits quasi-instantaneous behavior and its sign is negative in agreement with 2PA. The fact that  $n_2 < 0$  and  $\lambda_{\text{pump}} > \lambda_{\text{probe}}$  [see Fig. 2(a)] rules out coherent power transfer between probe and pump beams (“two-beam coupling” [2]) as an alternative to 2PA as a mechanism for the probe amplitude variations.

Having established that temporal peaks in both  $\Delta A$  and  $\Delta\phi$  are coming from intrinsic electronic response of GaAs we finally turn to the delay between amplitude  $\Delta T/T$  and phase  $\phi$  responses that can be clearly seen in Figs. 3(a) and 3(b). As shown in Figs. 3(c) and 3(d) the magnitude of the delays are  $\delta T_{xx} \approx 100 \text{ fs}$  and  $\delta T_{xy} \approx 120 \text{ fs}$  for the parallel and crossed configurations, respectively. These values correspond to  $\delta T \cdot \Delta_{\text{gap}}/h \approx 30$ , which is consistent with the simplified model in Fig. 1 (including the sign). Most importantly the lags do not show any dependence on pump intensity in line with the dispersive analysis. This observation rules out alternative lagging mechanisms based on nonlinear phenomena. This observation of a clear intensity-independent lag between phase and amplitude responses in agreement with theoretical expectations is the main result of this paper.

#### IV. DISCUSSION

As mentioned above, in addition to the quasi-instantaneous peak, the phase response in Fig. 3 features a prominent long-lived “tail” that is building up over the course several picoseconds and stays constant for the entire accessible delay

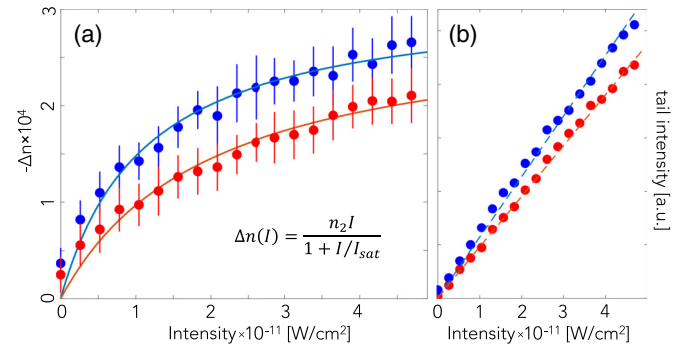


FIG. 4. (a) Dependence of the effective instantaneous nonlinear refractive index  $\bar{\delta n}$  on peak pump intensity  $I_0$  (see text). Solid lines are fits including saturation intensity  $I_{\text{sat}} = 0.8 \times 10^{11} \text{ W/cm}^2$ ,  $\bar{\delta n}(I_0) = \bar{n}_2 I_0 / (1 + I_0 / I_{\text{sat}})$ . (b) Pump intensity dependence of the long-lived tail in the phase response in Fig. 3. In both panels the blue and red markers/lines correspond to  $xx$  and  $xy$  configurations, respectively.

range (see Fig. 6 in the Appendix). This tail clearly has a different origin as compared to the to the main peak. This can already be seen in the different dependence on pump intensity  $I_p$  between the peak and tail shown in Fig. 4. While the tail grows linearly with  $I_p$ , the peak exhibits a clear saturation with a characteristic intensity  $I_{\text{sat}} = 8 \times 10^{10} \text{ W/cm}^2$  (both  $xx$  and  $yy$ ). Next, extended lifetime implies that the tail owes its origin to some real excitations produced by the pump. The linear pump intensity dependence [(Fig. 4(b)) excludes nonlinear absorption mechanisms, such as 2PA, as the possible origin of the tail; thermo-optic effect should also be excluded, since thermo-optic coefficient in GaAs is positive [21]. With these considerations we believe the most likely origin of the tail is the photo-excitation of the deep defect states (as previously reported in [22]) followed by long-lived low-density electron-hole plasma formation. The low plasma frequency ensures negative contribution to the refractive index.

The presence of the tail illustrates the usefulness of time-resolved methods for determining the intrinsic electronic Kerr index  $n_2$ . Our value for nonlinear Kerr index at  $\lambda = 1028 \text{ nm}$  can be compared to a significantly larger one obtained in an earlier measurement at  $1060 \text{ nm}$  by Said *et al.* [23]. The origin of the discrepancy likely lies in the fact that in [23] they were using  $40 \text{ ps}$  laser pulses. At such timescales the tail will be giving an integrated contribution [see Figs. 3(a) and 3(b)] that will overwhelm the intrinsic instantaneous response. Therefore we disregard this number in the present study and rely on the values obtained with ultrashort pulses as in [20].

Finally, apart from the amplitude-phase lag the physics described above have further practical important implications. Indeed, the common case of a self-Kerr effect of a beam can be thought of as a special case of Eq. (5) with  $t_0 = 0$ . In this case as these equations indicate, the Kerr changes of both amplitude and phase will be systematically less than what one would expect without taking dispersive effects in account. Here we use the full expression for  $\bar{n}_2(\omega, \Omega)$  to evaluate the correction factors  $F_{\text{ph}}$  and  $F_{\text{amp}}$  for phase and amplitude changes respectively, which we define as

$$F_{\text{ph}} = |\Delta\phi_{\text{max}}/\Delta\phi_0 - 1|, \quad F_{\text{amp}} = |\Delta A_{\text{max}}/\Delta A_0 - 1|$$

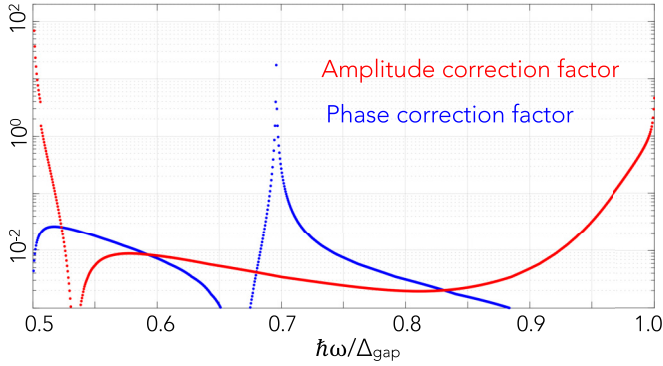


FIG. 5. Dispersion-induced renormalization factors for amplitude (blue) and phase (purple) response of a Kerr-active medium (see text).

where  $\Delta\phi_{\max}$  and  $\Delta A_{\max}$  are the maximum phase and amplitude changes achievable by tuning  $t_0$ ; while  $\Delta\phi_0$  and  $\Delta A_0$  are the same quantities evaluated at  $t_0 = 0$ . These correction factors show by how much the Kerr response of a system can exceed the nominal values calculated without regard to the dispersive effects discussed above. The correction factors calculated as function of frequency for a generic pulse duration  $\tau = \tau_1 = 70$  fs is plotted in Fig. 5. As can be seen from the plot, the response renormalization becomes significant near the  $\text{Re}\{n_2\}$  sign-switching wavelength and near single- and two-photon resonances.

## V. CONCLUSIONS

To summarize, we propose a procedure to extend the dispersive analysis of Sheik-Bahae *et al.* [16,17] to the situations where the pump intensity cannot be approximated as quasistatic and show that the resulting causal Kerr susceptibility  $\chi_K(t, t', t'')$  can be directly related to the dispersive Kerr index  $\bar{n}_2(\omega, \Omega)$ . We find that dispersive effects can lead to significant modifications in phase and amplitude dynamics, which lead to a significant underestimation of the peak Kerr response of a nonlinear medium. Our results shed light on the fundamental effects of causality for the ultrafast nonlinear phenomena and pave way for their efficient application.

## ACKNOWLEDGMENTS

The work was supported by the Institute of Science and Technology Austria (ISTA). We thank Prof. John M. Dudley, Dr. Ugur Sezer, and Dr. Artem Volosniev for valuable discussions.

## APPENDIX

### 1. Experimental details

The GaAs sample used in this study is a 675- $\mu\text{m}$  thick, (100)-oriented, semi-insulating GaAs wafer (Freiberger Compound Materials GmbH). An amplified femtosecond laser system (*Light Conversion* Pharos) coupled with an optical parametric amplifier (*Light Conversion* Orpheus) is used as the principal laser source. The laser produces a train of pulses centered at 1028 nm with a repetition rate of 3 kHz, pulse duration of 290 fs and a pulse energy of 2 mJ. A small part

of the beam (5%) is sent to the Mach-Zehnder interferometer (MZI) through a variable attenuator consisting of a half-wave plate (HWP) and a Glan-Taylor polarizer; the remaining part of the beam pumps the optical parametric amplifier with a tunable output wavelength.

In this paper, the fundamental wavelength of 1028 nm is used as a probe while the 1060 nm idler output from the optical parametric amplifier is used as the pump beam. The pump wavelength was chosen such that it is nearly degenerate with probe, but is still different enough to be effectively separable from the latter by means of a spectral filter. The delay between pump and probe is controlled with a motorized linear stage. Both pump and probe pass through a set of wave-plates and polarizers to attenuate their respective powers and to clean the polarizations. The pump beam is then passed through an additional HWP in order to control its polarization. The pump and probe beams are loosely focused and spatially overlapped in the sample in a slightly noncollinear arrangement. Care was taken to make sure that the probe diameter [ $D_{\text{probe}} \approx 120 \mu\text{m}$  ( $1/e^2$ )] at the sample position is considerably smaller than that of the pump, the latter being evaluated as  $D_{\text{pump}} \approx 360 \mu\text{m}$  ( $1/e^2$ ) by means of razor-blade method. This is made to ensure that pump intensity is a well-defined quantity. The probe light leaving the output port of MZI passes through a  $1030 \pm 5$  nm bandpass filter and the resulting interferograms are recorded by a CCD camera (*PointGrey Research Inc.* CM3-U3-50S5M). The pump intensity was tuned in a broad range up to  $\sim 5 \times 10^{11}$  W/cm<sup>2</sup>, while the probe intensity was kept fixed at  $I_{\text{probe}} = 4 \times 10^6$  W/cm<sup>2</sup>.

The pump-induced change in complex refractive index is obtained through measuring the changes in the phase  $\phi(t_0)$  and amplitude  $|K(t_0)|$  of the corresponding Fourier peak as function of delay  $t_0$  between the pump and probe beams,

$$\begin{aligned} \Re\{\Delta n(t_0)\} &= \frac{\lambda}{2\pi L} \{\phi(t_0) - \phi(-\infty)\}, \\ \Im\{\Delta n(t_0)\} &\approx -\frac{\lambda}{2\pi L} \frac{|K(t_0)| - |K(-\infty)|}{|K(-\infty)|}, \end{aligned}$$

here “ $t = -\infty$ ” we mean a large enough negative delay when probe beam precedes the pump. The delay between the pump and probe pulses  $t_0$  is controlled by a fast motorized delay stage (Newport LTLMS800). To extract the time dependence of transient changes to  $n_2$  the stage is moved incrementally and an interferogram is recorded for each position of the stage. In order to avoid the detrimental effects of mechanical vibrations, for every delay stage position we record two consecutive interferograms: one at the actual desired position and the other at a fixed reference position predating pump arrival (“ $t = -\infty$ ”). The changes in both the amplitude and phase are found from the difference between the two interferograms. Given the high speed of the delay stage (500 mm/s) this method helps minimize the effect of the low frequency noise coming from mechanical deformations of MZI.

### 2. Signal for large pump-probe delay values

Here we study the temporal behavior of the “tail” whose onset is shown in Fig. 3 of the main text. A long scan has been performed and the Fig. 6 shows that the signal remains virtually unchanged for pump-probe delays of multiple tens

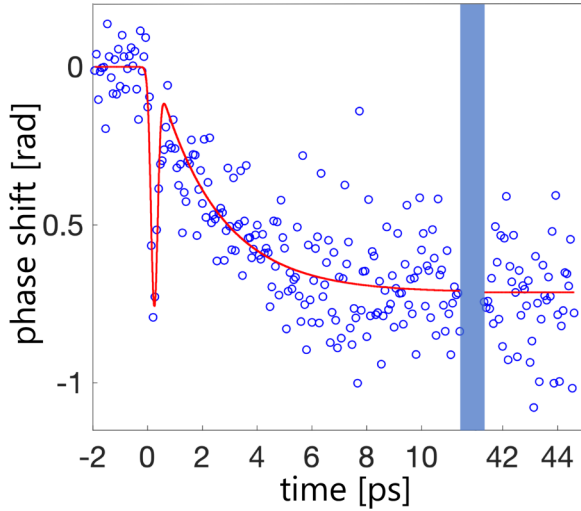


FIG. 6. Pump-induced phase shift in GaAs sample as a function of pump-probe delay in an extended range.

of picoseconds. On the one hand, the fact the feature has a long lifetime means that the pump is producing real excitation, on the other, the pump photon energy of 1.17 eV, which is less than GaAs band-gap energy of about  $\Delta_{\text{GaAs}} \approx 1.5$  eV. The most obvious mechanism for absorption of sub-gap photons is two-photon absorption. However, this is ruled out by the scaling of the “tail” magnitude with pump intensity, which is linear, as can be seen in Fig. 4(b) of the main text. Here it might be important to clarify that this ruled-out real two-photon absorption is different from the virtual two-photon process giving rise to the coherent feature around  $t = 0$  that is the main subject of this paper. In the ruled-out two-photon process both photons would be coming from the pump beam, while in the  $t = 0$  virtual process one of the two photons is still provided by the pump while the other comes from the probe. Therefore we can conclude the observed “tail” signal must originate from single-photon absorption. While such process is nominally prohibited for subgap frequencies, this is only strictly true for ideal samples. In realistic materials there always exist deep donor levels, which can be excited with sub-gap photons. Similar processes have been reported previously in, e.g., Ref. [22].

### 3. Propagation of nearly degenerate pulses around $\lambda \approx 1 \mu\text{m}$ in GaAs

The difference in wavelength between the pump and probe implies that the two have different group velocities. This gives rise to the walk-off between pulses as they propagate through the sample, which means that the effective interaction length is smaller than sample thickness  $L$ . In the main text the effective change in refractive index is defined as  $\delta\bar{n} = (\Delta\phi/2\pi) \cdot (\lambda/L)$  from which the effective Kerr index is inferred as  $\delta\bar{n} = \bar{n}_2 I_0$ ,  $I_0$  being (peak) pump pulse intensity. Now, since the interaction length is in fact less than  $L$ ,  $\bar{n}_2$  always underestimates the actual Kerr index value. Here we perform a simulation of pump-probe pulse interaction in order to find out the extent to which  $\bar{n}_2$  falls behind  $n_2$  in magnitude when walk-off effects are taken into account. For the present

purpose we ignore absorption effects and go ahead with the standard equations for cross-phase modulation [24],

$$\frac{\partial A_j}{\partial z} + \beta_{1j} \frac{\partial^2 A_j}{\partial t^2} = in_2(\omega_j/c) \{f_{jj}|A_j|^2 + 2f_{jk}|A_k|^2\} A_j, \quad (\text{A1})$$

here the index  $j = 1, 2$  corresponds to the probe and pump pulses respectively;  $A_j(z, t)$  is the amplitude of  $j$ th pulse,  $z$  and  $t$  being the distance in the propagation direction and time respectively;  $\beta_{1j}$  and  $\beta_{2j}$  are the group velocity and GVD coefficients of  $j$ th pulse respectively; while  $f_{jk}$  is the overlap coefficient (having the meaning of the inverse of the effective overlap area) between the  $j$ th and  $k$ th pulses with modal distributions  $F_j(x, y)$ ,

$$f_{jk} = \frac{\int dx dy |F_j(x, y)|^2 |F_k(x, y)|^2}{(\int dx dy |F_j(x, y)|^2)(\int dx dy |F_k(x, y)|^2)}.$$

To compare with experiment the quantity of interest is  $A_1(L, t)$  that is the amplitude of probe field at the exit from the sample. To mimic the experimental setup in which we measure the shifts of interference patterns, we first calculate the amplitude  $A_1^0(L, t)$  after the sample in the absence of pump pulse. We will use it as a reference pulse playing the role of the pulse in the reference arm of the Mach-Zehnder interferometer in Fig. 2 of the main text. Next, we add the pump pulse  $A_2$ . The temporal position of the pump in relation with probe (pump-probe delay) is kept as a free parameter  $\tau_{\text{delay}}$  and for each value, we calculate the field amplitude of the probe pulse that has interacted with the pump at the exit of the sample  $A_1(L, t, \tau_{\text{delay}})$ .

In order to simulate the experimental interference pattern we calculate the “interference” between sample field  $A_1(L, t, \tau_{\text{delay}})$  the reference field  $A_1^0(L, t, \phi) \equiv A_1^0(L, t) \exp(i\phi)$  retarded by some variable phase  $\phi$ . The meaning of this phase is to simulate the actual interference pattern where, e.g., depending on the point on the screen the probe and reference beams have different mutual phase dictated by the wavelength of the beams and their intersection angle. It is this space-dependent phase that gives rise to the interference pattern. With this in mind we calculate the interference term in the cumulative intensity  $G(\phi)$  as

$$G(\phi, \tau_{\text{delay}}) = \int dt ((A_1(L, t, \tau_{\text{delay}}))^* A_1^0(L, t) \exp(i\phi) + A_1(L, t, \tau_{\text{delay}}) (A_1^0(L, t))^* \exp(-i\phi)). \quad (\text{A2})$$

In Fig. 7 we plot  $G(\phi, \tau_{\text{delay}})$  with and without group-index-mismatch effects taken into account. Here we use the following parameters:

- (i) Wavelength:  $\lambda_{\text{probe}} = 1030$  nm (probe);  $\lambda_{\text{pump}} = 1060$  nm (pump)
- (ii) Pulse duration (pump and probe):  $\tau_{\text{pulse}} = 270$  fs
- (iii) Spot area (Gaussian profile):  $A_{\text{eff1}} = \pi(45 \times 10^{-6})^2$  m<sup>2</sup> (probe);  $A_{\text{eff1}} = \pi(180 \times 10^{-6})^2$  m<sup>2</sup> (pump)
- (iv) Sample thickness:  $L = 700 \mu\text{m}$ ; Kerr nonlinear refractive index:  $n_2 = 1.2 \times 10^{-19}$  m<sup>2</sup>/W
- (v) Group refractive index:  $n_{g1} = 3.9899$  (probe);  $n_{g2} = 3.9254$  (pump) (Ref. [25])

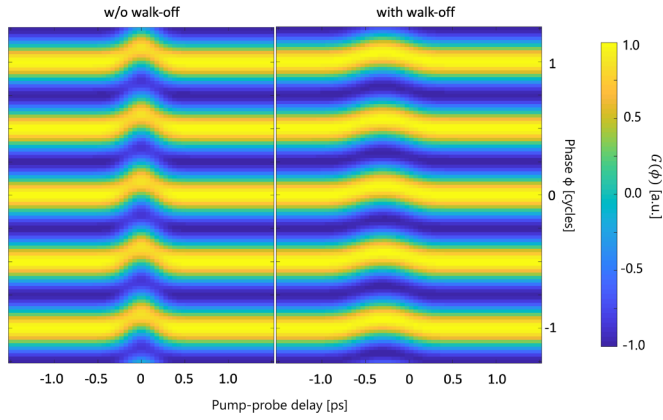


FIG. 7. “Interference patterns” as a function of delay between pump and probe with (right) and without (left) group index mismatch between pump and probe pulses taken into account. Simulation was carried out at peak pump intensity  $I_0 = 9.8 \times 10^{14} \text{ W/m}^2$  and  $n_2 = 1.2 \times 10^{-19} \text{ m}^2/\text{W}$ .

(vi) GVD coefficient:  $\beta_{11} = 4.5532$  (probe);  $\beta_{12} = 3.8172$  (pump) (Ref. [25]).

As can be seen, introducing the walk-off does not give rise to an orders-of magnitude change in peak phase shift. To see this more clearly, in Fig. 8 we plot  $G(\phi, \tau_{\text{delay}})$  with  $\tau_{\text{delay}}$  fixed at maximum phase shift position. The peak phase shifts with and without walk-off compare as 0.65 to 1. It is in place to mention that the peak phase  $\Delta\phi \approx 1.2$  rad shift in this simulation for  $I_0 \approx 10^{11} \text{ W/cm}^2$  is seemingly smaller than the experimentally measured  $\Delta\phi_{\text{exp}} \approx 0.5$  rad; however, this discrepancy is actually due to the fact that our simulation does not take saturation effects into account (see Fig. 4 in the main text).

When walk-off effects are taken into account, the phase shift as can be seen in Fig. 8 is reduced by about a factor of 2. This means that the ignoring the walk-off underestimates Kerr index only by the same factor of 2. This justifies the usage of the effective Kerr index in the main text for the purpose of the order-of-magnitude estimate of its actual value.

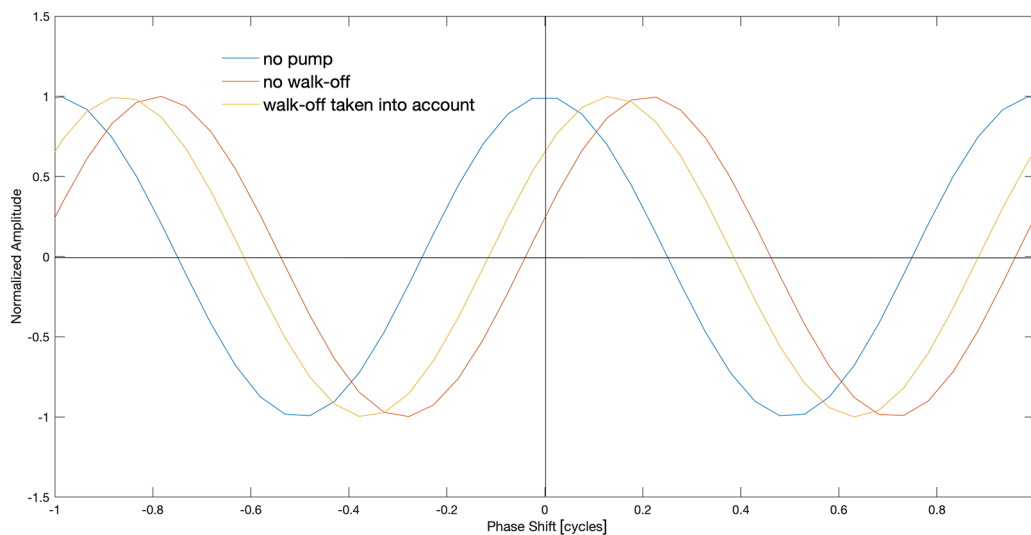


FIG. 8. Comparison of the “interference patterns” between the probe and reference beams in the absence of pump (blue).

#### 4. Dispersive relations for quasi-instantaneous off-resonant electron-mediated Kerr effect

*Relationship between Kerr susceptibility  $\chi^K$  and nonlinear refractive index.* The goal of this section is to establish the relation between the function  $f(t)$  and nonlinear Kerr index  $n_2$ . At this point it is important to mention the fact that the result of the previous section is that taking spatial dispersion into account does not affect the behavior of propagating fields at given frequencies in a qualitative manner. This observation justifies limiting one’s attention only to their time dependence as was done throughout the analysis in the main text in general and in Eq. (2) of the main text in particular. This approximation, however, does not affect to the validity of Eq. (4) of the main text. To demonstrate it we will derive this equation here without neglecting the spatial dependence of the fields. Reformulating Eq. (2) of the main text as a relationship between the local field values we can rewrite it as

$$\delta E_{\text{NL}}(x, t) = \int_{-\infty}^t dt' E_{\text{pr}}(x, t') \times \int_{-\infty}^t dt'' \delta\chi^K(x, t, t', t'') I_p(x, t''), \quad (\text{A3})$$

here  $E_{\text{pr}}(x, t)$  is the incident (probe) field at location with coordinate  $x$  at the moment  $t$ ;  $\delta E_{\text{NL}}(x, t)$  is the field generated at that locality due to nonlinear Kerr effect; and  $\delta\chi^K(x, t, t', t'')$  is the Kerr susceptibility of the infinitesimal region of the nonlinear medium surrounding the point  $x$  (see Fig. 9). Since we limit our attention only to the third-order nonlinear processes, we can assume that once created at point  $x$ ,  $\delta E_{\text{NL}}(x, t)$  does not participate in any further nonlinear interactions and simply propagates towards the exit of the sample at  $x = L$ . The full nonlinear response of the sample  $\Delta E_{\text{NL}}$  can then be found by summing the contributions of all  $\delta E_{\text{NL}}$  taking care to account for the phase acquired on the way there,

$$\Delta E_{\text{NL}}(L, t) = \int_0^L \delta E_{\text{NL}}(x, t) e^{i(L-x)\omega(\omega)/c}, \quad (\text{A4})$$

$$E_{pr}(x, t) = E_{pr}^\omega \exp(-i\omega t + i\omega n(\omega)x/c)$$

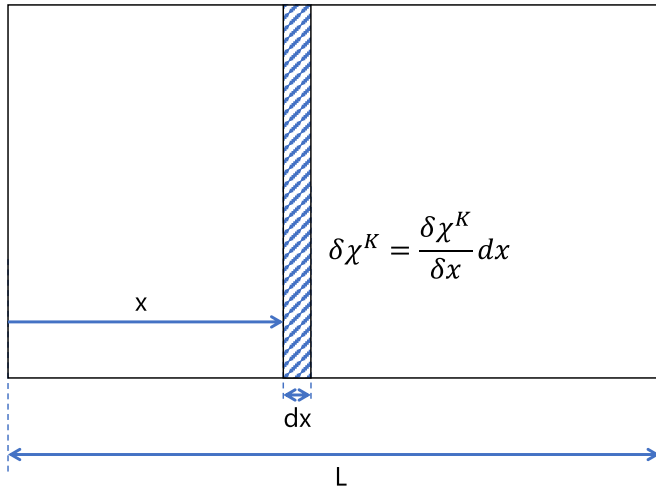


FIG. 9. Flat wave-front monochromatic wave  $E_{pr}(x, t)$  propagating in an extended medium of thickness  $L$  and phase refractive index  $n(\omega)$  along  $x$  axis;  $\delta\chi^K$  is the differential susceptibility of a sliver of thickness  $dx$  at position  $x$ .

where we need to insert here Eq. (A3), with  $E_{pr}(x, t) = E_{pr}^\omega \exp(-i\omega t + ix\frac{\omega n(\omega)}{c})$ ; Eq. (3) of the main text must also be modified for a thin slice of thickness  $dx$  to use here in the form

$$\begin{aligned} \delta\chi^K(t, t', t'') &= \delta f(t - t') \delta(t' - t'') \equiv \left( \frac{f(t - t')}{L} dx \right) \delta(t' - t''). \end{aligned} \quad (A5)$$

In order to relate  $\chi^K$  to nonlinear refractive index  $n_2$  we can apply the expressions above to the special case of monochromatic probe field  $E_{pr}(x, t) = E_{pr}^\omega \exp(-i\omega t + ix\frac{\omega n(\omega)}{c})$  and constant pump intensity  $I_p(x, t) = I_0 = const$ . Then nonlinear field generated at position  $x$  is

$$\begin{aligned} \delta E_{NL}(x, t) &= \int_{-\infty}^t dt' E_{pr}(x, t') \int_{-\infty}^t dt'' \chi^K(t, t', t'') I_p(x, t'') \\ &= \int_{-\infty}^t E_{pr}(x, t') \int_{-\infty}^t dt'' \delta(t' - t'') \\ &\quad \times \delta f(t - t') I_p(x, t'') \\ &= \int_{-\infty}^t E_{pr}(x, t') \delta f(t - t') I_p(x, t') \\ &= I_0 \int_{-\infty}^{+\infty} dt' E_{pr}(x, t') \delta f(t - t'), \end{aligned} \quad (A6)$$

here we have changed the upper integration limit by noticing that  $f(t) = 0$  for  $t < 0$ . Entering the explicit expression for  $E_{pr}(x, t)$  and  $\delta f(t)$  from above we get for the total nonlinear correction to the probe field  $\Delta E_{NL}$ ,

$$\begin{aligned} \Delta E_{NL}(L, t) &= \Delta E_{NL}^\omega e^{-i\omega t} \\ &= \int_0^L \delta E_{NL}(x, t) e^{i\frac{\omega n(\omega)}{c}(L-x)} \end{aligned}$$

$$\begin{aligned} &= I_0 \int_0^L dx \int_{-\infty}^{+\infty} dt' E_{pr}^\omega e^{-i\omega t + ix\frac{\omega n(\omega)}{c} + i\frac{\omega n(\omega)}{c}(L-x)} \\ &\quad \times f(t - t')/L \\ &= I_0 E_{pr}^\omega e^{i\frac{\omega n(\omega)L}{c}} \int_{-\infty}^{+\infty} dt' f(t - t') e^{-i\omega t}, \end{aligned} \quad (A7)$$

from which it follows immediately that the amplitude of monochromatic nonlinear field  $\Delta E_{NL}^\omega$  at the position of sample exit ( $x = L$ ) is related to the amplitude of monochromatic probe field amplitude at the same position  $E_{pr}^\omega(L) \equiv E_{pr}^\omega e^{i\frac{\omega n(\omega)L}{c}}$  simply as

$$\Delta E_{NL}^\omega = I_0 E_{pr}^\omega(L) f(\omega), \quad (A8)$$

where  $f(\omega) = \int dt f(t) \exp(-i\omega t)$ . On the other hand, when  $I_p(t) = const$ , the nonlinear correction  $\Delta E_{NL}$  can also be expressed in terms of nonlinear refractive index  $n_2$ . Indeed, when an incident field  $E_{pr}(x = 0, t) = E_{pr}^\omega \exp(-i\omega t)$  is incident on a sample with a refractive index  $\tilde{n}(\omega) = n(\omega) + \tilde{n}_2(\omega, \Omega) I_0$ , the total field at the exit of it is equal to

$$\begin{aligned} E_{out}(L, t) &= E_{out}^\omega(L) e^{-i\omega t} \\ &= E_{pr}^\omega e^{i\omega t - i\omega[n(\omega) + \tilde{n}_2(\omega, \Omega) I_0]L/c} = \\ &= E_{pr}^\omega e^{i\omega t - i\omega n(\omega)L/c} \cdot e^{i\omega \tilde{n}_2(\omega, \Omega) I_0 L/c}, \end{aligned} \quad (A9)$$

where we introduce  $\tilde{n}_2(\omega, \Omega)$  as the nonlinear refractive index describing the Kerr effect between probe at frequency  $\omega$  and pump at frequency  $\Omega$ . The nonlinear response of the sample can be defined as the difference between  $E_{out}(L, t)$  calculated with and without  $I_0$ ,

$$\begin{aligned} \Delta E_{NL}(L, t) &= E_{pr}^\omega e^{i\omega t - i\omega n(\omega)L/c} \cdot (e^{i\omega \tilde{n}_2(\omega, \Omega) I_0 L/c} - 1) \\ &\approx E_{pr}^\omega(L, t) \cdot \left( i \frac{\omega \tilde{n}_2(\omega, \Omega) I_0 L}{c} \right), \end{aligned} \quad (A10)$$

from which it follows that

$$\Delta E_{NL}^\omega \approx E_{pr}^\omega(L) \cdot \frac{i\omega \tilde{n}_2(\omega, \Omega) I_0 L}{c}. \quad (A11)$$

Comparing this with Eq. (A7) we immediately arrive at

$$f(\omega) \approx \frac{i\omega \tilde{n}_2(\omega, \Omega) L}{c}, \quad (A12)$$

which is nothing but Eq. (4) of the main text.

*Application to the case of two Gaussian pulses.* To see implications of the formalism described in the previous paragraph, let us consider the case when both pump and probe have a Gaussian profile shifted relative to each by  $t_0$ ,

$$I_p(t) = I_0 \exp(-2(t - t_0)^2/\tau_1^2), \quad (A13)$$

$$E_{pr}(t) = E_{pr} \exp(-t^2/\tau^2) \cos(\omega_0 t), \quad (A14)$$



then

$$\begin{aligned} \delta E_{\text{NL}}(t, t_0) = & \int dt_1 f(t - t_1) I_p(t_1) E_{\text{pr}}(t_1) \propto I_0 E_{\text{pr}} \int \frac{d\omega}{2\pi} f(\omega) \left\{ \exp \left[ \frac{(2t_0/\tau_1^2 + i(\omega + \omega_0)/2)^2 - \frac{2t_0^2}{\tau_1^2} - i\omega t}{2/\tau_1^2 + 1/\tau^2} \right] \right. \\ & \left. + \exp \left[ \frac{(2t_0/\tau_1^2 + i(\omega - \omega_0)/2)^2 - \frac{2t_0^2}{\tau_1^2} - i\omega t}{2/\tau_1^2 + 1/\tau^2} \right] \right\}. \end{aligned} \quad (\text{A15})$$

In practice, in order to characterize a rapidly oscillating pulse  $E(t)$  one can interfere it with some reference pulse  $E_{\text{ref}}(t, \theta)$  with same central frequency as the characterized pulse, and a controllable phase  $\theta$  relative to it. The measured signal is the total energy of the mixed pulse  $\delta \mathcal{E}(\theta) \propto \int dt (E(t) + E_{\text{ref}}(t, \theta))^2$ . If the phase or amplitude of  $E(t)$  changes for some reason, this will in general affect  $\delta \mathcal{E}$ . More specifically, the phase and amplitude shifts of  $E(t)$  are correspondingly proportional to

$$\begin{aligned} \Delta A & \propto \delta \mathcal{E}(\theta = 0) - \delta \mathcal{E}(\theta = \pi), \\ \Delta \phi & \propto \delta \mathcal{E}(\theta = \pi/2) - \delta \mathcal{E}(\theta = -\pi/2). \end{aligned} \quad (\text{A16})$$

Indeed, as an illustration one can imagine two laser beams being interfered at a screen while intersecting at some finite angle. Then if the amplitude of one of the beams has changed, this will affect the contrast ratio of the interference pattern, i.e., difference in intensity between the maximum (when mutual phase difference  $\theta = 0$ ) and minimum intensity positions (destructive interference, phase  $\theta = \pi$ ). Likewise, the change in phase in one of the beams results in the shift of the interference pattern as a whole. The magnitude of the latter can be found as the difference in intensity changes at the positions of the highest spatial gradient of intensity on the pattern, i.e., when  $\theta = \pm\pi/2$ .

The relevant part of  $\delta \mathcal{E}(\theta)$  is the one that comes from the mixing of  $E(t)$  and  $E_{\text{ref}}(t)$ ,

$$\delta \mathcal{E}_{\text{mix}}(\theta) = 2 \int dt E(t) E_{\text{ref}}(t). \quad (\text{A17})$$

Note that since  $\theta$  dependence of  $\delta \mathcal{E}(\theta)$  is entirely due to  $\delta \mathcal{E}_{\text{mix}}(\theta)$  one can substitute the former for the latter in Eq. (A16).

In our experiment  $E(t) = E_{\text{pr}} + \delta E_{\text{NL}}(t)$  with  $E_{\text{pr}}$  and  $\delta E_{\text{NL}}(t)$  defined in Eqs. (A14) and (A15) respectively; and  $E_{\text{ref}}(t, \theta) = E_{\text{pr}}(t + \theta/\omega_0)$ . Now putting these into  $\delta \mathcal{E}_{\text{mix}}(\theta)$  we write

$$\begin{aligned} \delta \mathcal{E}_{\text{mix}}(t_0, \theta) = & \text{const} \cdot E_{\text{pr}}^2 I_0 \int_{-\infty}^{+\infty} dt \int_{-\infty}^{+\infty} \frac{d\omega}{2\pi} f(\omega) \left[ e^{-i^2/\tau^2 + i\omega_0 t + i\theta} + e^{-i^2/\tau^2 - i\omega_0 t - i\theta} \right] \\ & \cdot \left[ \exp \left\{ \frac{[2t_0/\tau_1^2 + i(\omega + \omega_0)/2]^2}{2/\tau_1^2 + 1/\tau^2} - \frac{2t_0^2}{\tau_1^2} - i\omega t \right\} + \exp \left\{ \frac{[2t_0/\tau_1^2 + i(\omega - \omega_0)/2]^2}{2/\tau_1^2 + 1/\tau^2} - \frac{2t_0^2}{\tau_1^2} - i\omega t \right\} \right]. \end{aligned} \quad (\text{A18})$$

Dropping the oscillating terms (rotating wave approximation) and integrating over  $t$  gives

$$\begin{aligned} \delta \mathcal{E}_{\text{mix}}(t_0, \theta) \approx & \text{const} \cdot E_{\text{pr}}^2 I_0 \int \frac{d\omega}{2\pi} f(\omega) \cdot \\ & \cdot \left[ \exp \left\{ -\frac{2t_0^2}{\tau_1^2} - \left( \frac{\omega - \omega_0}{2} \right)^2 \tau^2 + i\theta + \frac{[2t_0/\tau_1^2 + i(\omega - \omega_0)/2]^2}{2/\tau_1^2 + 1/\tau^2} \right\} + (\omega_0 \rightarrow -\omega_0, \theta \rightarrow -\theta) \right]. \end{aligned} \quad (\text{A19})$$

This integral can be evaluated by using steepest descent method. However, noticing that as long as  $\tau \gg h/\Delta_{\text{gap}}$ ,  $f(\omega)$  is a slowly varying function as compared to the Gaussian in the rectangular brackets above. Therefore the latter can be approximated as delta function and the integral can then be evaluated trivially to give approximately

$$\begin{aligned} \delta \mathcal{E}_{\text{mix}}(t_0, \theta) & \\ \propto & E_{\text{pr}}^2 I_0 \cdot e^{-(t_0/\bar{\tau})^2} \cdot [f(\omega_0 + i\eta)e^{i\theta} + f(-\omega_0 + i\eta)e^{-i\theta}]. \end{aligned} \quad (\text{A20})$$

Here we introduced  $\bar{\tau}^2 = (\tau^2 + \tau_1^2)/2$  and  $\eta = t_0/\bar{\tau}^2$ . Now substituting this into Eq. (A16) and using Eq. (A12) we can write down the amplitude  $\Delta A$  and phase response  $\Delta \phi$  as a function of pump-probe delay  $t_0$  in terms of nonlinear refrac-

tive index  $n_2(\omega)$  as

$$\begin{aligned} \Delta \phi(t_0) & \propto I_0 \cdot [-n_2(\omega_0 + i\eta) + n_2(-\omega_0 + i\eta)], \\ \Delta A(t_0) & \propto I_0 \cdot i[n_2(\omega_0 + i\eta) + n_2(-\omega_0 + i\eta)]. \end{aligned} \quad (\text{A21})$$

For typical pulses  $\eta \ll \omega_0$ , therefore the expressions above can be evaluated to a good precision by means of Taylor expansion near  $\pm\omega_0$ . In general  $n_2(\omega)$  is a complex-valued function of  $\omega$  on a complex plane; however, given that away from the branching points at  $\omega_0 = 0.5\Delta_{\text{gap}}$  and  $\omega_0 = \Delta_{\text{gap}}$   $n_2(\omega)$  analytical and thus satisfies Cauchy-Riemann conditions. Then it is sufficient to know how  $n_2(\omega)$  depends on  $\omega$  on real axis alone to find  $n_2$  values in its immediate

vicinity,

$$\begin{aligned} \Delta A(t_0) &\propto I_0 \operatorname{Im}\{n_2(\omega_0)\} \\ &\cdot \exp\left[-\frac{1}{\bar{\tau}^2}\left(t_0 - \frac{\partial(\operatorname{Re}\{n_2\})/\partial\omega}{2\operatorname{Im}\{n_2\}}\right)^2\right], \\ \Delta\phi(t_0) &\propto I_0 \operatorname{Re}\{n_2(\omega_0)\} \\ &\cdot \exp\left[-\frac{1}{\bar{\tau}^2}\left(t_0 + \frac{\partial(\operatorname{Im}\{n_2\})/\partial\omega}{2\operatorname{Re}\{n_2\}}\right)^2\right], \end{aligned} \quad (\text{A22})$$

the derivatives here are evaluated at  $\omega = \omega_0$ . In order to proceed further we need to know the functional dependence of the nonlinear refractive index  $n_2(\omega)$  on frequency.

*Frequency dependence of nonlinear refractive index.* In this paragraph we write down for the record the expression for the nonlinear refractive index as calculated by means of the dispersive approach of Sheik-Bahae *et al.* in Refs. [16,17]. Generally speaking nonlinear refractive (Kerr) index is a function of both pump- and probe frequencies,  $\Omega$  and  $\omega$ , respectively. In the cited papers the authors notice that when pump intensity is constant  $I_p(t) = I_0$ , the total Kerr-modified refractive index of the medium can still be treated as linear index when used to describe the propagation of the probe beam. This means that, among other things, the correction to the refractive index  $\delta n(\omega) = n_2(\omega, \Omega)I_0$  must satisfy Kramers-Kronig relations,

$$\operatorname{Re}\{n_2(\omega, \Omega)\} = \frac{1}{\pi} \int_{-\infty}^{+\infty} \frac{\operatorname{Im}\{n_2(\omega', \Omega)\}}{\omega' - \omega} d\omega'. \quad (\text{A23})$$

Imaginary part of the Kerr index corresponds to pump-induced absorption of the probe beam. In the simplest case this can happen due to two-photon absorption (2PA). The magnitude for 2PA was calculated for a direct-gap semiconductor in Refs. [17,26]. Being only interested in the frequency dependence of  $n_2$  we write down the result of that study as

$$\begin{aligned} \operatorname{Im}\{n_2(\omega, \Omega)\} &= \operatorname{const} \cdot \frac{(\omega + \Omega - \Delta)^{3/2}}{\omega^2 \Omega^2} \left(\frac{1}{\omega} + \frac{1}{\Omega}\right)^2 \\ &\cdot \Theta(\omega + \Omega - \Delta), \end{aligned} \quad (\text{A24})$$

where  $\Theta(x)$  is the Heaviside step function. Since in Eq. (A23) we integrate along the entire real axis, we need to fix what  $n_2$  is for negative  $\omega$ . The reality of  $n_2(t - t')$  requires that  $n_2(\omega) = n_2^*(-\omega)$ . Therefore, the 2PA part of  $n_2$  should

read

$$\begin{aligned} \operatorname{Im}\{n_2^{2\text{PA}}(\omega, \Omega)\} &= \frac{\operatorname{const}}{\omega^4 \Omega^4} \{(\omega + \Omega - \Delta)^{3/2}(\omega + \Omega)^2 \cdot \Theta(\omega + \Omega - \Delta) \\ &+ (\Omega - \omega - \Delta)^{3/2}(\Omega - \omega)^2 \cdot \Theta(\Omega - \omega - \Delta)\}. \end{aligned} \quad (\text{A25})$$

Further, as will be clear below, we need to also symmetrize the above expression with respect to  $\Omega$ . These new terms achieved by substituting  $\Omega \rightarrow -\Omega$  can be identified with Raman contribution to  $n_2$ ,

$$\begin{aligned} \operatorname{Im}\{n_2^{2\text{PA}+\text{Raman}}(\omega, \Omega)\} &= \frac{\operatorname{const}}{\omega^4 \Omega^4} \{(\omega + \Omega - \Delta)^{3/2}(\omega + \Omega)^2 \cdot \Theta(\omega + \Omega - \Delta) \\ &+ (\Omega - \omega - \Delta)^{3/2}(\Omega - \omega)^2 \cdot \Theta(\Omega - \omega - \Delta) \\ &+ (\omega - \Omega - \Delta)^{3/2}(\omega - \Omega)^2 \cdot \Theta(\omega - \Omega - \Delta) \\ &+ (-\Omega - \omega - \Delta)^{3/2}(-\Omega - \omega)^2 \cdot \Theta(-\Omega - \omega - \Delta)\}. \end{aligned} \quad (\text{A26})$$

Now we can perform the integral in Eq. (A23); however, in addition to the physical branching points at  $\omega = \pm(\Delta \pm \Omega)$  that correspond to certain two-photon absorption thresholds, there is an unphysical singularity at  $\omega = 0$ . As discussed in Ref. [17] this is an artifact of the derivation of two-photon absorption probability by means of dipole ( $\mathbf{A} \cdot \mathbf{p}$ ) approximation. At low frequencies this singularity is canceled by taking into account the omitted diamagnetic term  $\mathbf{A}^2$ . Knowing that singularity at  $\omega = 0$  is fictitious, we can simply amend the expression above with a proper counterterm that will remove the divergence at  $\omega = 0$ .

An inspection of the expression for nondegenerate two-photon absorption above reveals that it is symmetric in  $\omega$  and  $\Omega$ . This is natural given how it is derived. What it means, however, is that to recover proper  $\omega$  dependence of  $n_2$ , one should also include the counter terms to remove the singularity at  $\Omega = 0$ . Then one finally would need to make sure that counter terms in  $\omega$  do not diverge at  $\omega = 0$  and vice versa. Adding everything up, and performing the Kramers-Kronig integration in Eq. (A23) we can write down the full expression for nondegenerate  $n_2$ ,

$$\begin{aligned} n_2^{2\text{PA}+\text{Raman}}(\omega, \Omega) &\propto \frac{\Delta^{9/2}}{\omega^4 \Omega^4} \left\{ (\Delta - \omega - \Omega)^{3/2}(\omega + \Omega)^2 + (\Delta + \omega - \Omega)^{3/2}(\Omega - \omega)^2 + (\Delta - \omega + \Omega)^{3/2}(\omega - \Omega)^2 + (\Delta + \Omega + \omega)^{3/2}(-\Omega - \omega)^2 \right. \\ &- 2\Omega^2(\Delta - \Omega)^{3/2} \left[ 1 + \frac{\omega^2}{\Omega^2} - \frac{3\omega^2}{\Omega(\Delta - \Omega)} + \frac{3}{8} \frac{\omega^2}{(\Delta - \Omega)^2} \right] - 2\Omega^2(\Delta + \Omega)^{3/2} \left[ 1 + \frac{\omega^2}{\Omega^2} + \frac{3\omega^2}{\Omega(\Delta + \Omega)} + \frac{3}{8} \frac{\omega^2}{(\Delta + \Omega)^2} \right] \\ &- 2\omega^2(\Delta - \omega)^{3/2} \left[ 1 + \frac{\Omega^2}{\omega^2} - \frac{3\Omega^2}{\omega(\Delta - \omega)} + \frac{3}{8} \frac{\Omega^2}{(\Delta - \omega)^2} \right] - 2\omega^2(\Delta + \omega)^{3/2} \left[ 1 + \frac{\Omega^2}{\omega^2} + \frac{3\Omega^2}{\omega(\Delta + \omega)} + \frac{3}{8} \frac{\Omega^2}{(\Delta + \omega)^2} \right] \\ &\left. + 4\Delta^{3/2}(\omega^2 + \Omega^2) + 9 \frac{\omega^2 \Omega^2}{\Delta^{1/2}} \right\}, \end{aligned} \quad (\text{A27})$$

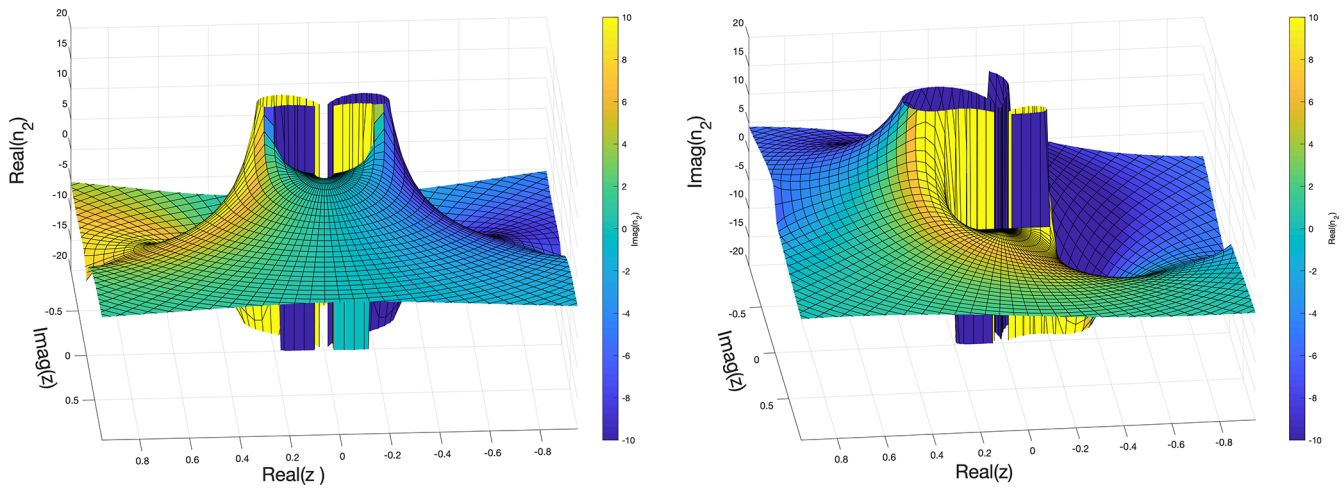


FIG. 10. Real (left) and imaginary (right) parts of  $n_2(\omega, \Omega)$  as a function of complex  $z = \omega/\Delta$  based of Eq. (A27). Here we took  $\Omega = 0.8\Delta$ .

here both  $\omega$  and  $\Omega$  are understood as complex variables. The real and imaginary parts of  $n_2$  are plotted in Fig. 10. In the degenerate limit  $\omega = \Omega$  the above expression can be checked to coincide with the functional dependence of  $n_2(\omega)$  given in [17].

- 
- [1] A. M. Zheltikov, In search of lost time: Attosecond physics, petahertz optoelectronics, and quantum speed limit, *Phys. Usp.* **64**, 370 (2021).
- [2] R. W. Boyd, *Nonlinear Optics*, 3rd ed. (Academic Press, Burlington, 2008).
- [3] J.-C. Diels and W. Rudolph, *Ultrashort Laser Pulse Phenomena*, 2nd ed. (Academic Press, Burlington, 2006).
- [4] T. Y. Chang, Fast self-induced refractive index changes in optical media: A survey, *Opt. Eng.* **20**, 220 (1981).
- [5] M. Bunge, *Causality and Modern Science* (Routledge, London, 2017).
- [6] J. S. Toll, Causality and the dispersion relation: Logical foundations, *Phys. Rev.* **104**, 1760 (1956).
- [7] R. de L. Kronig, On the theory of dispersion of x-rays, *J. Opt. Soc. Am.* **12**, 547 (1926).
- [8] K. H. A., La diffusion de la lumiere par les atomes, *Atti Cong. Intern. Fisica (Transactions of Volta Centenary Congress) Como* **2**, 545 (1927).
- [9] L. Rouleau, J.-F. Deü, A. Legay, and F. L. Lay, Application of Kramers-Kronig relations to time-temperature superposition for viscoelastic materials, *Mech. Mater.* **65**, 66 (2013).
- [10] J. Luo, X. Liang, Y. Zhang, C. Liang, H. Yassine, G. Leroy, J.-C. Carru, and M. Mascot, Application of the Kramers-Kronig relationships in the electrochemical impedance models fit, *J. Solid State Electrochem.* **25**, 2225 (2021).
- [11] R. Lovell, Application of Kramers-Kronig relations to the interpretation of dielectric data, *J. Phys. C* **7**, 4378 (1974).
- [12] T. Harter, C. Füllner, J. N. Kemal, S. Ummethala, J. L. Steinmann, M. Brosi, J. L. Hesler, E. Bründermann, A.-S. Müller, W. Freude *et al.*, Generalized Kramers-Kronig receiver for coherent terahertz communications, *Nat. Photonics* **14**, 601 (2020).
- [13] D. M. Roessler, Kramers-Kronig analysis of reflection data, *Br. J. Appl. Phys.* **16**, 1119 (1965).
- [14] H. M. Nussenzveig, *Causality and Dispersion Relations* (Academic Press, New York, 1972).
- [15] H. W. Bode, *Network Analysis and Feedback Amplifier Design* (D. van Nostrand, New York, 1945).
- [16] M. Sheik-Bahae, D. J. Hagan, and E. W. Van Stryland, Dispersion and band-gap scaling of the electronic Kerr effect in solids associated with two-photon absorption, *Phys. Rev. Lett.* **65**, 96 (1990).
- [17] D. C. Hutchings, M. Sheik-Bahae, D. J. Hagan, and E. W. V. Stryland, Kramers-krönig relations in nonlinear optics, *Opt. Quantum Electron.* **24**, 1 (1992).
- [18] K.-E. Peiponen, V. Lucarini, J. J. Saarinen, and E. Vartiainen, Kramers-Kronig relations and sum rules in nonlinear optical spectroscopy, *Appl. Spectrosc.* **58**, 499 (2004).
- [19] K.-E. Peiponen and J. J. Saarinen, Generalized Kramers-Kronig relations in nonlinear optical- and THz-spectroscopy, *Rep. Prog. Phys.* **72**, 056401 (2009).
- [20] W. C. Hurlbut, Y.-S. Lee, K. L. Vodopyanov, P. S. Kuo, and M. M. Fejer, Multiphoton absorption and nonlinear refraction of GaAs in the mid-infrared, *Opt. Lett.* **32**, 668 (2007).
- [21] F. G. D. Corte, G. Cocorullo, M. Iodice, and I. Rendina, Temperature dependence of the thermo-optic coefficient of InP, GaAs, and SiC from room temperature to 600 K at the wavelength of 1.5  $\mu\text{m}$ , *Appl. Phys. Lett.* **77**, 1614 (2000).
- [22] A. Bičiūnas, J. Adamonis, and A. Krotkus, Terahertz time-domain-spectroscopy system using a 1 micron wavelength laser and photoconductive components made from low-temperature-grown GaAs, *J. Infrared, Millimeter, Terahertz Waves* **33**, 183 (2011).
- [23] A. A. Said, M. Sheik-Bahae, D. J. Hagan, T. H. Wei, J. Wang, J. Young, and E. W. V. Stryland, Determination of bound-electronic and free-carrier nonlinearities in ZnSe, GaAs, CdTe, and ZnTe, *J. Opt. Soc. Am. B* **9**, 405 (1992).

- [24] G. Agrawal, *Nonlinear Fiber Optics* (Elsevier Science, Amsterdam, 2007).
- [25] T. Skauli, P. S. Kuo, K. L. Vodopyanov, T. J. Pinguet, O. Levi, L. A. Eyres, J. S. Harris, M. M. Fejer, B. Gerard, L. Becouarn, and E. Lallier, Improved dispersion relations for GaAs and applications to nonlinear optics, *J. Appl. Phys.* **94**, 6447 (2003).
- [26] M. Sheik-Bahae, D. Hutchings, D. Hagan, and E. V. Stryland, Dispersion of bound electron nonlinear refraction in solids, *IEEE J. Quantum Electron.* **27**, 1296 (1991).